Analytical coupled-channel treatment of two-body scattering in the presence of three-dimensional isotropic spin-orbit coupling

Q. Guan and D. Blume

Analytical coupled-channels treatment of two-body scattering in the presence of three-dimensional isotropic spin-orbit coupling

Q. Guan[1] and D. Blume[1]

[1]*Department of Physics and Astronomy, Washington State University, Pullman, Washington 99164-2814, USA*
(Dated: February 1, 2017)

It is shown that the single-particle spin-orbit coupling terms, which—in the cold atom context—are associated with synthetic gauge fields, can significantly and non-trivially modify the phase accumulation at small interparticle distances even if the length scale $(k_{so})^{-1}$ associated with the spin-orbit coupling term is significantly larger than the van der Waals length r_{vdW} that characterizes the two-body interaction potential. A theoretical framework, which utilizes a generalized local frame transformation and accounts for the phase accumulation analytically, is developed. Comparison with numerical coupled-channels calculations demonstrates that the phase accumulation can, to a very good approximation, be described over a wide range of energies by the free-space scattering phase shifts—evaluated at a scattering energy that depends on k_{so}—and the spin-orbit coupling strength k_{so}.

PACS numbers:

The tunability of low-energy scattering parameters such as the s-wave scattering length a_s and p-wave scattering volume V_p by means of application of an external magnetic field in the vicinity of a Feshbach resonance [1] has transformed the field of ultracold atom physics, providing experimentalists with a knob to "dial in" the desired Hamiltonian. This tunability has afforded the investigation of a host of new phenomena including the BEC-BCS crossover [2, 3]. Most theoretical treatments of these phenomena are formulated in terms of a few scattering quantities such as a_s and V_p, which properly describe the low-energy behavior of the two-body system.

The recent realization of spin-orbit coupled cold atom systems [4] is considered another milestone, opening the door for the observation of topological properties and providing a new platform with which to study scenarios typically encountered in condensed matter systems with unprecedented control [5–7]. An assumption that underlies most theoretical treatments of cold atom systems with synthetic gauge fields is that the spin-orbit coupling term, i.e., the Raman laser that couples the different internal states or the shaking of the lattice that couples different bands, leaves the atom-atom interactions "untouched". More specifically, mean-field treatments "simply" add the single-particle spin-orbit coupling term to the mean-field Hamiltonian and parameterize the atom-atom interactions via contact potentials with coupling strengths that are calculated for the two-body van der Waals potential without the spin-orbit coupling terms [7, 8].

Consistent with such mean-field approaches, most two-body scattering studies derive observables based on the assumption that the two-body Bethe-Peierls boundary condition, derived in the absence of single-particle spin-orbit coupling terms, remains unaffected by the spin-orbit coupling terms, provided an appropriate "basis transformation" is accounted for [9–16]. The underlying premise of these two-body and mean-field treatments is rooted in scale separation, which suggests that the free-space scattering length a_s and scattering volume V_p remain good quantities provided $(k_{so})^{-1}$ is larger than the two-body van der Waals length r_{vdW}. Indeed, model calculations for a square-well potential in the presence of three-dimensional isotropic spin-orbit coupling suggest that the above reasoning holds, provided $1/a_s$ and V_p are small [17].

This work revisits the question of how to obtain and parameterize two-body scattering observables in the presence of three-dimensional isotropic spin-orbit coupling. Contrary to what has been reported in the literature, our calculations for Lennard-Jones and square-well potentials show that the three-dimensional isotropic spin-orbit coupling terms can impact the phase accumulation in the small interparticle distance region where the two-body interaction potential cannot be neglected even if $(k_{so})^{-1}$ is notably larger than r_{vdW}. We observe non-perturbative changes of the scattering observables when k_{so} changes by a small amount. An analytical treatment, which reproduces the full coupled-channels results such as the energy-dependent two-body cross sections for the finite-range potentials with high accuracy, is developed. Our analytical treatment relies, as do previous treatments [9–13, 15–17], on separating the short- and large-distance regions. The short-distance Hamiltonian is treated by applying a gauge transformation, followed by a rotation, that "replaces" the **p**-dependent spin-orbit coupling term by an **r**- and **p**-independent diagonal matrix (**r** and **p** denote the relative position and momentum vectors, respectively). The diagonal terms, which can be interpreted as shifting the scattering energy in each channel, can introduce non-perturbative changes in the scattering observables for small changes in k_{so}, especially when V_p is large. We note that our derivation of the short-distance Hamiltonian, although similar in spirit, differs in subtle but important ways from what is presented in Ref. [10, 12].

Our analytical framework also paves the way for designing energy-dependent zero-range or δ-shell pseudo-

potentials applicable to systems with spin-orbit coupling. While energy-dependent pseudo-potentials have proven useful in describing systems without spin-orbit coupling [18, 19], generalizations to systems with spin-orbit coupling are non-trivial due to the more intricate nature of the dispersion curves. Our results suggest a paradigm shift in thinking about spin-orbit coupled systems with non-vanishing two-body interactions. While the usual approach is to assume that the short-distance behavior or the effective coupling strengths are not impacted by the spin-orbit coupling terms, our results suggest that they can be for specific parameter combinations. Even though our analysis is carried out for the case of three-dimensional isotropic spin-orbit coupling, our results point toward a more general conclusion, namely that spin-orbit coupling terms may, in general, notably modify the phase accumulation in the short-distance region.

We consider two particles with position vectors $\mathbf{r}_j$ and masses m_j ($j = 1$ and 2) interacting through a spherically symmetric two-body potential $V_{\mathrm{int}}(r)$ ($r = |\mathbf{r}_1 - \mathbf{r}_2|$). Both particles feel the isotropic spin-orbit coupling term with strength k_{so}, $V_{\mathrm{so}}^{(j)} = \hbar k_{\mathrm{so}} \mathbf{p}_j \cdot \boldsymbol{\sigma}^{(j)}/m_j$, where $\mathbf{p}_j$ denotes the canonical momentum operator of the jth particle and $\boldsymbol{\sigma}^{(j)}$ the vector that contains the three Pauli matrices $\boldsymbol{\sigma}_x^{(j)}$, $\boldsymbol{\sigma}_y^{(j)}$ and $\boldsymbol{\sigma}_z^{(j)}$ for the jth particle. Throughout, we assume that the expectation value of the total momentum operator $\mathbf{P}$ of the two-body system vanishes. In this case, the total angular momentum operator $\mathbf{J}$, $\mathbf{J} = \mathbf{l} + \mathbf{S}$, of the two-particle system commutes with the system Hamiltonian and the scattering solutions can be labeled by the quantum numbers J and M_J; M_J denotes the projection quantum number, $\mathbf{l}$ is the relative orbital angular momentum operator, and $\mathbf{S} = \hbar(\boldsymbol{\sigma}^{(1)} + \boldsymbol{\sigma}^{(2)})/2$.

Separating off the center of mass degrees of freedom, the relative Hamiltonian H for the reduced mass μ particle with relative momentum operator $\mathbf{p}$ can be written as a sum of the free-space Hamiltonian H_{fs} and the spin-orbit coupling term V_{so}, $H = H_{\mathrm{fs}} + V_{\mathrm{so}}$, where

$$H_{\mathrm{fs}} = \left[\frac{\mathbf{p}^2}{2\mu} + V_{\mathrm{int}}(r) \right] I_1 \otimes I_2 \qquad (1)$$

and $V_{so} = \hbar k_{so} \boldsymbol{\Sigma} \cdot \mathbf{p}/\mu$ with $\boldsymbol{\Sigma} = (m_2 \boldsymbol{\sigma}^{(1)} \otimes I_2 - m_1 I_1 \otimes \boldsymbol{\sigma}^{(2)})/M$. Here, I_j denotes the 2×2 identity matrix that spans the spin degrees of freedom of the jth particle and M the total mass, $M = m_1 + m_2$. For each (J, M_J) channel, the $\mathbf{r}$-dependent eigen functions $\Psi^{(J,M_J)}$ are expanded as [13, 15, 16]

$$\Psi^{(J,M_J)}(\mathbf{r}) = \sum_{l,S} r^{-1} u_{l,S}^{(J)}(k,r)|J, M_J; l, S\rangle, \qquad (2)$$

where the sum goes over $(l, S) = (0, 0)$ and $(1, 1)$ for $(J, M_J) = (0, 0)$ and over $(l, S) = (J, 0)$, $(J, 1)$, $(J-1, 1)$, and $(J+1, 1)$ for $J > 0$. In the $|J, M_J; l, S\rangle$ basis (using the order of the states just given), the scaled radial set of differential equations for fixed J and M_J reads

$\underline{h}^{(J)}\underline{u}^{(J)} = E\underline{u}^{(J)}$, where $\underline{h}^{(J)}$ [20] denotes the scaled radial Hamiltonian for a given J (note that the Hamiltonian is independent of the M_J quantum number). For $r > r_{\mathrm{max}}$, the interaction potential V_{int} can be neglected and $\underline{u}^{(J)}$ is matched to the analytic asymptotic $V_{\mathrm{int}} = 0$ solution [13, 15, 16]

$$\underline{u}^{(J)} \xrightarrow[r > r_{\mathrm{max}}]{} r \left(\underline{\mathcal{J}}^{(J)} - \underline{\mathcal{N}}^{(J)} \underline{K}^{(J)} \right), \qquad (3)$$

where $\underline{\mathcal{J}}^{(J)}$ and $\underline{\mathcal{N}}^{(J)}$ are matrices that contain the regular and irregular solutions for finite k_{so} (for $J = 0$ and 1, explicit expressions are given in Ref. [16]). Defining the logarithmic derivative matrix $\underline{\mathcal{L}}^{(J)}(r)$ through $(\underline{u}^{(J)})'(\underline{u}^{(J)})^{-1}$, where the prime denotes the partial derivative with respect to r, the K-matrix is given by

$$\underline{K}^{(J)} = \left[\left(r\underline{\mathcal{N}}^{(J)} \right)' - \underline{\mathcal{L}}^{(J)}(r) \left(r\underline{\mathcal{N}}^{(J)} \right)' \right] \times$$
$$\left[\left(r\underline{\mathcal{J}}^{(J)} \right)' - \underline{\mathcal{L}}^{(J)}(r) \left(r\underline{\mathcal{J}}^{(J)} \right) \right] \Big|_{r=r_{\mathrm{max}}}, \qquad (4)$$

the S-matrix by $\underline{S}^{(J)} = (\underline{I} + \imath\underline{K}^{(J)})(\underline{I} - \imath\underline{K}^{(J)})^{-1}$, where $\underline{I}$ denotes the identity matrix, and the cross sections by $\sigma_{\alpha\beta} = 2\pi|\underline{S}_{\beta\alpha}^{(J)} - \delta_{\alpha\beta}|^2/k_\alpha^2$, where α and β each take the values $1, 2, \cdots$.

In general, the K-matrix has to be determined numerically via coupled-channels calculations. In what follows, we address the question whether $\underline{K}$ can, at least approximately, be described in terms of the logarithmic derivative matrix of the free-space Hamiltonian H_{fs}. If the spin-orbit coupling term V_{so} vanished in the small r limit, one could straightforwardly apply a projection or frame transformation approach [21–24] that would project the inner small r solution, calculated assuming that V_{so} vanishes in the inner region, onto the outer large r solution, calculated assuming that V_{int} vanishes in the outer region [25]. The fact that V_{so} does not vanish in the small r limit requires, as we show below, a generalization of the frame transformation approach.

We start with the Hamiltonian H and define a new Hamiltonian $\tilde{H}$ through $T^{-1}HT$, where T is an operator to be determined. The solution $\tilde{\Psi}$ of the new Hamiltonian is related to the solution Ψ of H through $\tilde{\Psi} = T^{-1}\Psi$; here and in what follows we drop the superscripts "(J, M_J)" and "(J)" for notational convenience. The operator T reads RU, where $R = \exp(-\imath k_{\mathrm{so}} \boldsymbol{\Sigma} \cdot \mathbf{r})$; the form of U is introduced later. To calculate $H_R = R^{-1}HR$, we use

$$R^{-1}H_{\mathrm{fs}}R = H_{\mathrm{fs}} - V_{\mathrm{so}} - E_{\mathrm{so}}[\boldsymbol{\Sigma} \cdot \mathbf{r}, \boldsymbol{\Sigma} \cdot \nabla] + \mathcal{O}(\mathbf{r}) \quad (5)$$

and

$$R^{-1}V_{\mathrm{so}}R = V_{\mathrm{so}} + 2E_{\mathrm{so}}[\boldsymbol{\Sigma} \cdot \mathbf{r}, \boldsymbol{\Sigma} \cdot \nabla] + \mathcal{O}(\mathbf{r}), \qquad (6)$$

where $-\imath\hbar\nabla = \mathbf{p}$ and $E_{\mathrm{so}} = \hbar^2 k_{\mathrm{so}}^2/(2\mu)$ and where the notation $\mathcal{O}(\mathbf{r})$ indicates that terms of order r and higher are neglected ($\mathbf{r}$ "counts" as being of order r and $\mathbf{p}$ as being of order r^{-1}). Adding Eqs. (5) and (6) and neglecting the $\mathcal{O}(\mathbf{r})$ terms, we find that the spin-orbit coupling

term V_{so} is replaced by a commutator that arises from the fact that the operator $\mathbf{\Sigma} \cdot \mathbf{p}$ does not commute with the exponent of R,

$$H_R^{sr} = H_{fs} + E_{so} \left[\mathbf{\Sigma} \cdot \mathbf{r}, \mathbf{\Sigma} \cdot \nabla \right]. \tag{7}$$

Here, the superscript "sr" indicates that this Hamiltonian is only valid for small r [26].

Our goal is now to evaluate the second term on the right hand side of Eq. (7). Defining the scaled short-distance Hamiltonian h_R^{sr} through $r H_R^{sr} r^{-1}$ and expressing h_R^{sr} in the $|J, M_J; l, S\rangle$ basis, we find

$$\underline{h}_R^{sr} = \left(\frac{-\hbar^2}{2\mu} \frac{\partial^2}{\partial r^2} + V_{int}(r) \right) I_1 \otimes I_2 + \underline{\mathcal{V}} + \underline{\epsilon}, \tag{8}$$

where $\underline{\mathcal{V}}$ is a diagonal matrix with diagonal elements $\hbar^2 l(l+1)/(2\mu r^2)$. For $J = 0$, the matrix $\underline{\epsilon}$ is diagonal with diagonal elements $-3E_{so}$ and E_{so}. For $J > 0$, in contrast, the 11 and 22 elements are, in general, coupled:

$$\underline{\epsilon} = E_{so} \begin{pmatrix} -3 & c/M^2 & 0 & 0 \\ c/M^2 & -(\Delta M/M)^2 & 0 & 0 \\ 0 & 0 & d_1/M^2 & 0 \\ 0 & 0 & 0 & d_2/M^2 \end{pmatrix}, \tag{9}$$

where $\Delta M = m_1 - m_2$, $c = 2\sqrt{J(J+1)}(m_2^2 - m_1^2)$, $d_1 = -JM^2 - (J+1)\Delta M^2$, and $d_2 = 4m_1 m_2 - d_1$. Since the r-dependent 11 and 22 elements of $\underline{\mathcal{V}}$ are identical (recall $l = J$ for these two elements), the matrix $\underline{U}$, which is defined such that $\underline{U}^{-1} \underline{\epsilon} \underline{U}$ is diagonal, also diagonalizes $\underline{h}_R^{sr}$, i.e., the short-range Hamiltonian $\underline{\tilde{h}}_T^{sr} = \underline{U}^{-1} \underline{h}_R^{sr} \underline{U}$ is diagonal. This implies that the scaled radial short-distance Schrödinger equation $\underline{\tilde{h}}_T^{sr} \underline{v} = E\underline{v}$ can be solved using standard propagation schemes such as the Johnson algorithm [27]. This Schrödinger equation

differs from the "normal" free-space Schrödinger equation by channel-specific energy shifts. These shifts introduce a non-trivial modification of the phase accumulation in the short-distance region and—if a zero-range or δ-shell pseudo-potential description was used—of the boundary condition. While the energy shifts do, in many cases, have a negligible effect, our analysis below shows that they can introduce non-perturbative corrections in experimentally relevant parameter regimes. The channel-specific energy shifts are not taken into account in Ref. [12].

To relate the logarithmic derivative matrix $\underline{\tilde{\mathcal{L}}}^{sr}(r) = \underline{v}' \underline{v}^{-1}$ of the scaled short-distance Hamiltonian $\underline{\tilde{h}}_T^{sr}$ to the logarithmic derivative matrix $\underline{\mathcal{L}}(r)$, the "$T$-operation" needs to be "undone". Assuming that the short-distance Hamiltonian provides a faithful description, i.e., assuming that the higher-order correction terms can, indeed, be neglected for $r < r_{max}$, we obtain

$$\underline{\mathcal{L}}(r_{max}) \approx \left\{ \underline{T} \underline{\tilde{\mathcal{L}}}^{sr}(r) \underline{T}^{-1} - \underline{T} \left(\underline{T}^{-1} \right)' \right\} \Big|_{r=r_{max}}. \tag{10}$$

To illustrate the results, we focus on the $J = 0$ subspace. Denoting the usual free-space phase shifts at scattering energy $\hbar^2 k^2/(2\mu)$ for the interaction potential V_{int} for the s-wave and p-wave channels by $\delta_s(k)$ and $\delta_p(k)$, respectively, the short-range K-matrix $\underline{\tilde{K}}^{sr}$ for the Hamiltonian $\underline{\tilde{h}}_T^{sr}$ has the diagonal elements $\tan(\delta_s(k_s))$ and $\tan(\delta_p(k_p))$, where $\hbar^2 k_s^2/(2\mu) = E + 3E_{so}$ and $\hbar^2 k_p^2/(2\mu) = E - E_{so}$. If we now, motivated by the concept of scale separation, make the assumption that the phase shifts $\tan(\delta_s(k_s))$ and $\tan(\delta_p(k_p))$ are accumulated at $r = 0$ and correspondingly take the $r_{max} \to 0$ limit of Eq. (4) with $\underline{\mathcal{L}}^{(J)}$ given by the right hand side of Eq. (10), we obtain the following zero-range K-matrix,

$$\underline{K}^{zr} = -\frac{a_s(k_s)}{k_+ - k_-} \begin{bmatrix} k_+^2 & k_+ k_- \\ k_+ k_- & k_-^2 \end{bmatrix} - \frac{V_p(k_p)}{k_+ - k_-} \begin{bmatrix} k_+^2(k_- - k_{so})^2 & k_+ k_-(k_+ - k_{so})(k_- - k_{so}) \\ k_+ k_-(k_+ - k_{so})(k_- - k_{so}) & k_-^2(k_+ - k_{so})^2 \end{bmatrix}, \tag{11}$$

where $\hbar k_\pm = \pm\sqrt{2\mu(E + E_{so})} - \hbar k_{so}$.

To validate our analytical results, we perform numerical coupled-channels calculations. Since the wave function in the $J = 0$ subspace is anti-symmetric under the simultaneous exchange of the spatial and spin degrees of freedom of the two particles, the solutions apply to two identical fermions. The Schrödinger equation for the Lennard-Jones potential $V_{LJ}(r) = C_{12}/r^{12} - C_6/r^6$, with C_6 and C_{12} denoting positive coefficients, is solved numerically [28]. The solid lines in Figs. 1 and 2 show the partial cross section σ_{22} and the K-matrix element K_{22} as a function of k_{so} for vanishing scattering energy E for a two-body potential with large $a_s(0)$ and

large $V_p(0)$, respectively. The dashed lines show the results predicted by our zero-range model that accounts for the spin-orbit coupling induced energy shifts. This model provides an excellent description of the numerical results for the Lennard-Jones potential, provided the length $(k_{so})^{-1}$ associated with the spin-orbit coupling term is not too small compared to the van der Waals length r_{vdW}, where r_{vdW} is given by $(2\mu C_6/\hbar^2)^{1/4}$ (in Figs. 1 and 2, the largest $k_{so} r_{vdW}$ considered corresponds to 0.4913 and 0.4171, respectively).

The dash-dotted lines in Figs. 1 and 2 show σ_{22} and K_{22} for the zero-range model when we set the spin-orbit coupling induced energy shifts artificially to zero. In this
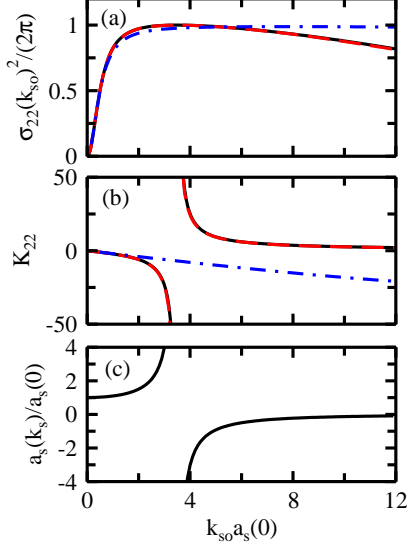
FIG. 1: (Color online) Large $a_s(0)$ case. The black solid line shows (a) the scaled partial cross section $\sigma_{22}(k_{\text{so}})^2/(2\pi)$ and (b) the K-matrix element K_{22} for $E = 0$ as a function of $k_{\text{so}}a_s(0)$ for the Lennard-Jones potential with $a_s(0)/r_{\text{vdW}} = 24.42$ and $V_p(0)/(r_{\text{vdW}})^3 = -0.2380$ (this potential supports two s-wave bound states in free space). The red dashed line shows the result for the zero-range model developed in this work [see Eq. (11)]; the numerical results for the Lennard-Jones potential and the model are indistinguishable on the scale shown. To illustrate the importance of the energy shifts, the blue dash-dotted line shows the results for the zero-range model that artificially neglects the energy shifts. The solid line in (c) shows the scaled energy-dependent s-wave scattering length $a_s(k_s)/a_s(0)$, where $\hbar^2 k_s^2 = 6\mu E_{\text{so}}$.
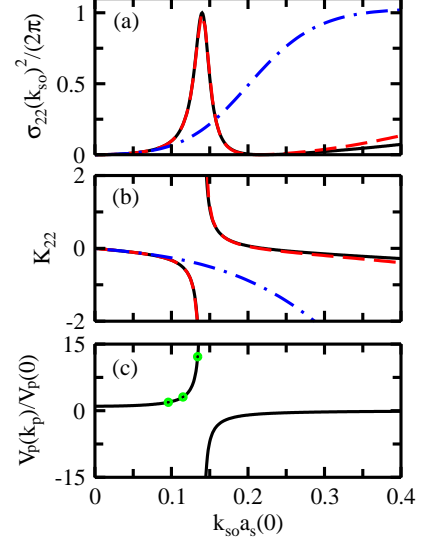

FIG. 2: (Color online) Large $V_p(0)$ case. The black solid line shows (a) the scaled partial cross section $\sigma_{22}(k_{\text{so}})^2/(2\pi)$ and (b) the K-matrix element K_{22} for $E = 0$ as a function of $k_{\text{so}}a_s(0)$ for the Lennard-Jones potential with $a_s(0)/r_{\text{vdW}} = 0.9591$ and $V_p(0)/(r_{\text{vdW}})^3 = 26.61$, corresponding to $a_s(0)/(V_p(0))^{1/3} = 0.3213$ (this potential supports 4 four s-wave bound states in free space). The red dashed line shows the result for the zero-range model developed in this work [see Eq. (11)]; the model reproduces the numerical results excellently for $k_{\text{so}}a_s(0) \lesssim 0.3$. The blue dash-dotted line shows the results for the zero-range model that artificially neglects the energy shifts. The solid line in (c) shows the scaled energy-dependent p-wave scattering volume $V_p(k_p)/V_p(0)$, where $\hbar^2 k_p^2 = -2\mu E_{\text{so}}$. The green circles mark three of the four $k_{\text{so}}a_s(0)$ values considered in Fig. 4.

case, the divergence in the K_{22} matrix element at finite k_{so} is not reproduced. For large $a_s(0)$ [see Fig. 1(a)], the model without energy shifts introduces deviations at the few percent level in the cross section σ_{22}. For large $V_p(0)$ [see Fig. 2(a)], in contrast, the model without the energy shifts provides a quantitatively and qualitatively poor description of the cross section σ_{22} even for relatively small k_{so} ($k_{\text{so}}a_s(0) \gtrsim 0.05$). Figures 1(c) and 2(c) demonstrate that the divergence of the K_{22} matrix element occurs when the free-space scattering length $a_s(k_s)$, calculated at energy $3E_{\text{so}}$, or the free-space scattering volume $V_p(k_p)$, calculated at energy $-E_{\text{so}}$, diverge. We find that this occurs roughly when $a_s(0)k_{\text{so}} \approx 10$ and $(V_p(0))^{1/3}k_{\text{so}} \approx 0.21$; we checked that this holds quite generally, i.e., not only for the parameters considered in the figures. In Figs. 1(c) and 2(c), the "critical" k_{so} values correspond to $k_{\text{so}}r_{\text{vdW}} = 0.1423$ and $k_{\text{so}}r_{\text{vdW}} = 0.1462$, respectively. For comparison, using the k_{so} value for the one-dimensional realization of Ref. [4] and assuming $r_{\text{vdW}} = 100a_0$, one finds $k_{\text{so}}r_{\text{vdW}} \approx 0.03$. This suggests that the phenomena discussed in the context of Figs. 1 and 2 should be relevant to future realizations of three-dimensional isotropic spin-orbit coupling exper-

iments.

To further explore the two-particle scattering properties in the presence of spin-orbit coupling for short-range potentials with large free-space scattering volume $V_p(0)$, Figs. 3(a) and 3(b) show the partial cross section σ_{22} as a function of the scattering energy $-E_{\text{so}} \leq E \leq 0$ and $0 \leq 0 \leq 400E_{\text{so}}$, respectively, for $a_s(0)/(V_p(0))^{1/3} = 0.3213$ and $a_s(0)k_{\text{so}} = 0.07673$. The results for the Lennard-Jones potential (dashed line) and square-well potential (solid line) are essentially indistinguishable on the scale shown. To assess the accuracy of our zero-range model, we focus on the Lennard-Jones potential and compare the numerically determined partial cross section $(\sigma_{22})^{\text{exact}}$ with the partial cross section $(\sigma_{22})^{\text{zr}}$ predicted using Eq. (11). Solid lines in Figs. 3(c) and 3(d) show the normalized difference Δ, defined through $\Delta = |(\sigma_{22})^{\text{zr}} - (\sigma_{22})^{\text{exact}}|/(\sigma_{22})^{\text{exact}}$. The deviations are smaller than 1.3% for the scattering energies considered. Neglecting the spin-orbit coupling induced energy shifts in our zero-range model and calculating the normalized difference, we obtain the dashed lines in Figs. 3(c) and 3(d). Clearly, the zero-range model provides a faith-
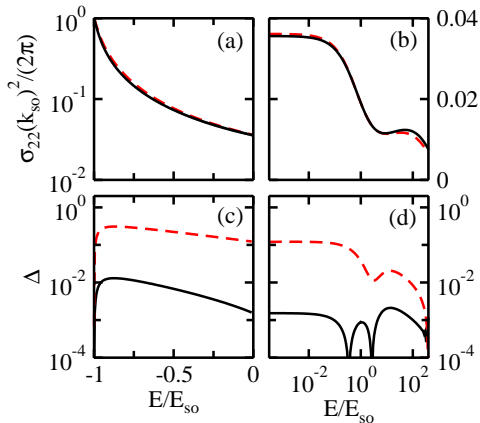
FIG. 3: (Color online) Large $V_p(0)$ case. (a) and (b): The red dashed and black solid lines show the scaled partial cross section $\sigma_{22}(k_{\mathrm{so}})^2/(2\pi)$ for the Lennard-Jones and square-well potential, respectively, as a function of the scattering energy E. For both potentials, we have $a_s(0)/(V_p(0))^{1/3} = 0.3213$ [$V_p(0) > 0$] and $k_{\mathrm{so}}a_s(0) = 0.07673$. The length scale associated with the spin-orbit coupling is notably larger than the range of the potential ($k_{\mathrm{so}}r_{\mathrm{vdW}} = 0.08$ for the Lennard-Jones potential and $k_{\mathrm{so}}r_{\mathrm{sw}} = 0.07676$ for the square-well potential). (c) and (d): The solid and dashed lines show the normalized difference Δ (see text) between the cross section for the Lennard-Jones potential and the zero-range model, obtained using Eq. (11), and between that for the Lennard-Jones potential and the zero-range model that neglects the spin-orbit coupling induced energy shifts, respectively. The zero-range model derived in this work (solid line) provides an excellent description (the deviations are smaller than 1.3 % for the data shown) over the entire energy regime. Panels (a) and (c) cover negative E (linear scale) while panels (b) and (d) cover positive E (logarithmic scale)].

ful description of the full coupled-channels data for the Lennard-Jones potential only if the spin-orbit coupling induced energy shifts are included.

Figure 4 demonstrates that the non-quadratic single-particle dispersion relations have a profound impact on the low-energy scattering observables for a large free-space scattering volume. Specifically, the lines in Fig. 4 show the numerically obtained partial cross section σ_{22} as a function of the scattering energy for the same Lennard-Jones potential as that used in Figs. 2 and 3 for four different spin-orbit coupling strengths, namely $k_{\mathrm{so}}r_{\mathrm{vdW}} = 0.1, 0.12, 0.14$ and 0.146 [Fig. 3 used $k_{\mathrm{so}}r_{\mathrm{vdW}} = 0.08$; three of the four k_{so} values considered in Fig. 4 are marked by circles in Fig. 2(c)]. Figure 4 shows that the partial cross section depends sensitively on the spin-orbit coupling strength k_{so}. This can be understood by realizing that a change in the spin-orbit coupling strength leads to a significant change of the k_{so}-dependent scattering volume $V_p(k_p)$.

This paper revisited two-body scattering in the presence of single-particle interaction terms that lead, in the absence of two-body interactions, to non-quadratic
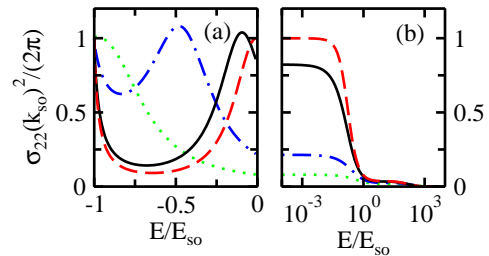

FIG. 4: (Color online) Scaled partial cross section $\sigma_{22}(k_{\mathrm{so}})^2/(2\pi)$ for the Lennard-Jones potential with $a_s(0)/(V_p(0))^{1/3} = 0.3213$ ($V_p(0) > 0$) and $a_s(0)/r_{\mathrm{vdW}} = 0.9591$ for four different k_{so} [the green dotted, blue dash-dotted, black solid, and red dashed lines correspond to $k_{\mathrm{so}}r_{\mathrm{vdW}} = 0.1$, $k_{\mathrm{so}}r_{\mathrm{vdW}} = 0.12$, $k_{\mathrm{so}}r_{\mathrm{vdW}} = 0.14$, and $k_{\mathrm{so}}r_{\mathrm{vdW}} = 0.146$, respectively] as a function of the scattering energy E [panel (a) covers negative E (linear scale) while panel (b) covers positive E (logarithmic scale)].

dispersion relations. Restricting ourselves to three-dimensional isotropic spin-orbit coupling terms and spin-independent central two-body interactions, we developed an analytical coupled-channels theory that connects the short- and large-distance eigenfunctions using a generalized frame transformation. A key, previously overlooked result of our treatment is that the gauge transformation that converts the short-distance Hamiltonian to the "usual form" (i.e., a form without linear momentum dependence) introduces channel-dependent energy shifts. These energy shifts were then shown to appreciably alter the low-energy scattering observables, especially in the regime where the free-space scattering volume is large. To illustrate this, the $(J, M_J) = (0, 0)$ channel was considered. Our framework provides the first complete analytical description that consistently accounts for all partial wave channels. Moreover, the first numerical coupled-channels results for two-particle Hamiltonian with realistic Lennard-Jones potentials in the presence of spin-orbit coupling terms were presented. The influence of the revised zero-range formulation put forward in this paper on two- and few-body bound states and on mean-field and beyond mean-field studies will be the topic of future publications.

[1] C. Chin, R. Grimm, P. Julienne, and E. Tiesinga, Feshbach resonances in ultracold gases, Rev. Mod. Phys. **82**, 1225 (2010).

[2] I. Bloch, J. Dalibard, and W. Zwerger, Many-body physics with ultracold gases, Rev. Mod. Phys. **80**, 885 (2008).

[3] Theory of ultracold atomic Fermi gases, S. Giorgini, L. P. Pitaevskii, and S. Stringari, Rev. Mod. Phys. **80**, 1215 (2008).

[4] Y.-J. Lin, K. Jiménez-García, and I. B. Spielman, Spin-orbit-coupled Bose-Einstein condensates, Nature (London) **471**, 83 (2011).

[5] J. Dalibard, F. Gerbier, G. Juzeliūnas, and P. Öhberg, Colloquium: Artificial gauge potentials for neutral atoms, Rev. Mod. Phys. **83**, 1523 (2011).

[6] V. Galitski and I. B. Spielman, Spin-orbit coupling in quantum gases, Nature **494**, 49 (2013).

[7] H. Zhai, Degenerate quantum gases with spin-orbit coupling: a review, Rep. Prog. Phys. **78**, 026001 (2015).

[8] H. Zhai, Spin-Orbit Coupled Quantum Gases, Int. J. Mod. Phys. B **26**, 1230001 (2012).

[9] X. Cui, Mixed-partial-wave scattering with spin-orbit coupling and validity of pseudopotentials, Phys. Rev. A **85**, 022705 (2012).

[10] P. Zhang, L. Zhang, and Y. Deng, Modified Bethe-Peierls boundary condition for ultracold atoms with spin-orbit coupling, Phys. Rev. A **86**, 053608 (2012).

[11] Z. Yu, Short-range correlations in dilute atomic Fermi gases with spin-orbit coupling, Phys. Rev. A **85**, 042711 (2012).

[12] L. Zhang, Y. Deng, and P. Zhang, Scattering and effective interactions of ultracold atoms with spin-orbit coupling, Phys. Rev. A **87**, 053626 (2013).

[13] H. Duan, L. You, and B. Gao, Ultracold collisions in the presence of synthetic spin-orbit coupling, Phys. Rev. A **87**, 052708 (2013).

[14] Y. -C. Zhang, S. -W. Song, W. -M. Liu, The confinement induced resonance in spin-orbit coupled cold atoms with Raman coupling, Sci. Rep. **4**, 4992 (2014).

[15] S.-J. Wang and C. H. Greene, General formalism for ultracold scattering with isotropic spin-orbit coupling, Phys. Rev. A **91**, 022706 (2015).

[16] Q. Guan and D. Blume, Scattering framework for two particles with isotropic spin-orbit coupling applicable to all energies, Phys. Rev. A **94**, 022706 (2016).

[17] Y. Wu and Z. Yu, Short-range asymptotic behavior of the wave functions of interacting spin-1/2 fermionic atoms with spin-orbit coupling: A model study, Phys. Rev. A **87**, 032703 (2013).

[18] D. Blume and C. H. Greene, Fermi pseudopotential approximation: Two particles under external confinement, Phys. Rev. A **65**, 043613 (2002).

[19] E. L. Bolda, E. Tiesinga, and P. S. Julienne, Effective-scattering-length model of ultracold atomic collisions and Feshbach resonances in tight harmonic traps, Phys. Rev. A **66**, 013403 (2002).

[20] Here and in what follows, underlined quantities are matrices.

[21] U. Fano, Stark effect of nonhydrogenic Rydberg spectra, Phys. Rev. A **24**, 619(R), (1981).

[22] D. A. Harmin, Theory of the Nonhydrogenic Stark Effect, Phys. Rev. Lett. **49**, 128 (1982).

[23] C. H. Greene, Negative-ion photodetachment in a weak magnetic field, Phys. Rev. A **36**, 4236 (1987).

[24] B. E. Granger and D. Blume, Tuning the Interactions of Spin-Polarized Fermions Using Quasi-One-Dimensional Confinement, Phys. Rev. Lett. **92**, 133202 (2004).

[25] S.-J. Wang, Ph.D thesis, Purdue University (2016).

[26] For equal masses, $H_R^{\rm sr}$ can be rewritten as $H_{\rm fs} + E_{\rm so}[-3 + (\mathbf{S}^2 - \mathbf{l} \cdot \mathbf{S})/\hbar^2]$. This expression highlights that the spin-orbit coupling Hamiltonian is of relativistic nature; moreover, it provides a simple means to evaluate the commutator.

[27] B. R. Johnson, The Multichannel Log-Derivative Method for Scattering Calculations, J. Comput. Phys. **13**, 445 (1973).

[28] F. Mrugała and D. Secrest, The generalized log-derivative method for inelastic and reactive collisions, J. Chem. Phys. **78**, 5954 (1983).